Pergamon

Neural Networks, Vol. 7, Nos. 6/7, pp. 883–894, 1994

0893-6080/94 $6.00 + .00

0893-6080(94)E0026-H

1994 SPECIAL ISSUE

Rules for the Cortical Map of Ocular Dominance and Orientation Columns

STEPHEN GROSSBERG AND STEVEN J. OLSON

Boston University

(*Received* 6 *October* 1993; *revised and accepted* 15 *February* 1994)

Abstract—*Three computational rules are sufficient to generate model cortical maps that simulate the interrelated structure of cortical ocular dominance and orientation columns: a noise input, a spatial band pass filter, and competitive normalization across all feature dimensions. The data of Blasdel from optical imaging experiments reveal cortical map fractures, singularities, and linear zones that are fit by the model. In particular, singularities in orientation preference tend to occur in the centers of ocular dominance columns, and orientation contours tend to intersect ocular dominance columns at right angles. The model embodies a universal computational substrate that all models of cortical map development and adult function need to realize in some form.*

Keywords—Visual cortex, Ocular dominance, Orientation columns, Band pass filter, Hypercolumns, Neural networks, Cortical maps, Cortical development.

1. INTRODUCTION

Since the classical work of Hubel and Wiesel (1974) many experimental neurobiologists have studied how two key structural attributes of striate visual cortex (V1) develop in the neonate and are functionally organized in the adult. These attributes are the ocular dominance columns in which visual inputs from the left and right eyes are juxtaposed to facilitate binocular vision, and the orientation columns in which oriented edges, textures, and shading in an image can selectively activate some cells more than others. The anatomical coordination of these attributes was first conceptualized in the hypercolumn model of Hubel and Wiesel (1974). Much subsequent experimental work has revealed a complex organization of these interwoven attributes of ocular dominance and orientation selectivity, one that includes a mesh of singularities, fractures, and linear zones. Blasdel (1992a,b) has described five general characteristics of ocular dominance and orientation maps:

1. there exist regions of smooth change in orientation preference (linear zones);
2. there exist rapid changes in orientation along one direction (fractures);
3. there exist regions at the centers of swirls of orientation preference in which all orientation preferences are present (singularities);
4. singularities tend to lie within the centers of the ocular dominance columns; and
5. linear zones intersect the edges of ocular dominance columns nearly orthogonally.

Figure 1 shows each of these five characteristics in a map of orientation preference and ocular dominance columns obtained by optical dye recordings.

Ocular dominance columns in V1 have been studied extensively in macaque monkeys with a wide variety of techniques. These methods include anatomical staining of the cortical afferents from one eye (Hubel, Wiesel, & LeVay, 1977); imaging the differential uptake of 2-deoxyglucose (2DG) in response to monocular stimulation (Hubel, Wiesel, & Stryker, 1978; Humphrey & Hendrickson, 1983; Tootel, Hamilton, Silverman, & Switkes, 1988); tracing retinal–cortical connectivity by injecting [^{3}H]proline into one eye (LeVay, Connolly, Houde, & Van Essen, 1985); and optical dye recordings of cortical response to monocular stimulation (Blasdel, 1992a,b; Blasdel & Salama, 1986; Obermayer & Blasdel, 1993). These studies reveal qualita-

Acknowledgements: The authors thank Eric Schwartz for helpful discussions on this topic. S.G. was supported in part by the Air Force Office of Scientific Research (AFOSR F49620-92-J-0499), the Advanced Research Projects Agency (ONR N00014-92-J-4015), and the Office of Naval Research (ONR N00014-91-J-4100). S.J.O. was supported in part by the Air Force Office of Scientific Research (AFOSR F49620-92-J-0334), British Petroleum (BP 89A-1204), the National Science Foundation (NSF IRI-90-24877), and the Office of Naval Research (ONR N00014-91-J-4100).

Requests for reprints should be sent to Dr. Stephen Grossberg, Boston University, Department of Cognitive and Neural Systems, 111 Cummington Street, Boston, MA 02215.

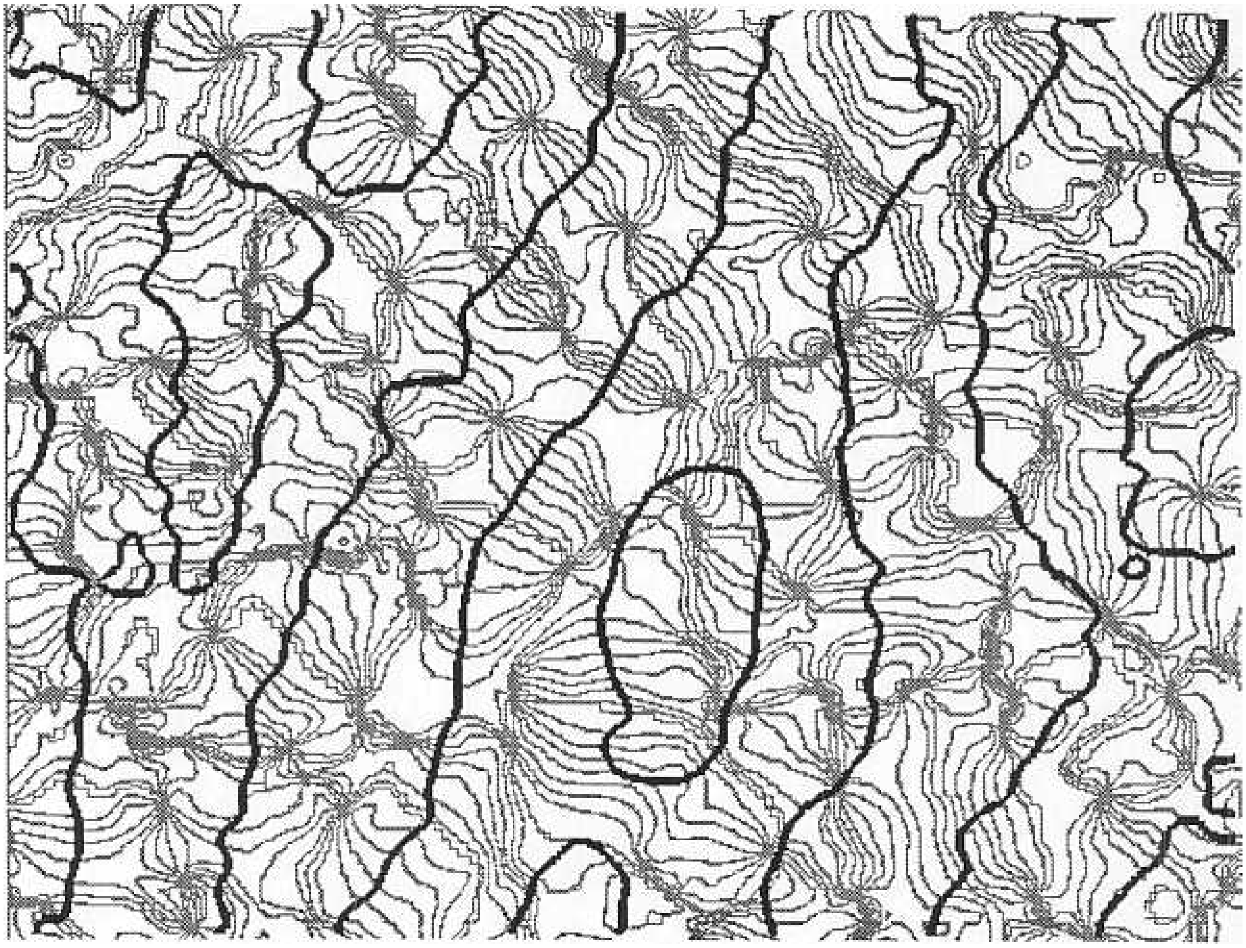

FIGURE 1. Characteristics of orientation and ocular dominance maps, revealed by optical imaging. Five key properties of cortical maps are illustrated: 1. regions of smooth change in orientation preference (linear zones); 2. regions in which orientation changes rapidly along one direction (fractures); 3. regions at the center of swirls of orientation where all orientations are present (singularities); 4. singularities tend to lie within the centers of ocular dominance columns; 5. linear zones tend to intersect ocular dominance columns nearly orthogonally. Reprinted with permission from Obermayer and Blasdel (1993).

tively and quantitatively similar observations of the columnar organization of eye preference columns.

Primate ocular dominance columns appear organized in long fairly regular bands or stripes. Stripes corresponding to regions of high preference for the right eye are interdigitated with stripes preferring the left eye. Although these stripes appear to have some global order, they are not perfectly uniform structures. Instead individual stripes exhibit many branches and "blind endings" (LeVay, Hubel, & Wiesel, 1975). Nevertheless, the stripes are sufficiently regular that it is sensible to compute the average stripe width. Hubel et al. (1977) estimated the width of a single stripe (which subserves a single eye) to be about 300–450 μm. In their 2DG study, Hubel, et al. (1978) corroborate this estimate. Using reconstructions of [^{3}H]proline injections studies, LeVay et al. (1985) report the slightly larger estimate of the width of a pair of stripes as 880 μm. Optical dye measurements confirm that the width of a pair of columns is on the order of 822 microns (Blasdel & Salama, 1986; Blasdel, 1992a,b; Obermayer & Blasdel, 1993).

In the macaque, Hubel and Wiesel (1974) estimate that orientation preference changes at a rate of about 281°/mm. This corresponds to a range of about 640 μm for a full sweep through 180° of preference. Studying 2DG uptake within macaque primary visual cortex in response to vertical stripes, Hubel et al. (1978) found a pattern of roughly interdigitated "swirling stripes with many bifurcations and blind endings" that are similar to the ocular dominance columns, but are less regular. They estimate that a pair of stripes subtends a cortical distance of about 570 μm. Stimulating with alternating horizontal and vertical lines reduces the spacing of the patches by a factor of 2 which confirms the notion that there are distinct spatial representations of different orientations on the cortical surface.

Optical dye recordings of macaque cortex (Blasdel & Salama, 1986; Blasdel, 1992a,b; Obermayer & Blasdel, 1993) confirm the earlier estimates of orientation column size. They find that the typical spacing between regions of similar orientation (or more technically, the dominant wavelength in the images of orientation preference) is about 679 μm. This value is quite close to the values estimated earlier from electrophysiological and 2DG studies. In addition to a confirmation of the size of the orientation columns, the optical dye recordings reveal the overall structure of orientation columns in monkey cortex. Orientation preference columns seem to be arranged in a "pinwheel" pattern around centers with little or no orientation selectivity. Application of a gradient operator to these images reveals the existence of regions of rapid orientation change, or "fractures," which tend to connect neighboring centers.

2. NEURAL NETWORK MODELS

This explosion of neural data has led to a correspondingly vigorous development of neural network models to simulate and explain them. Grossberg (1972, 1976a,b), von der Malsburg (1973), and Willshaw and von der Malsburg (1976) introduced key associative and competitive mechanisms for map formation, followed by a rapidly increasing number of contributions in the 1980s and beyond by Bienenstock, Cooper, and Munro (1982), Kohonen (1989), Linsker (1986), and others (see Table 1). These models have tended to mix two goals: to understand the functional organization of columnar structures in primate visual cortex, and to understand how this columnar organization forms through a self-organizing developmental process.

Although each of these neural models shares a number of features in common, such as associative learning and competitive decision rules, their very numbers and continued proliferation indicates that no one model has yet definitively been accepted. To facilitate this process, the present article identifies three computational properties that all models need to possess in order to explain data concerning the adult organization of ocular dominance and orientation columns. These properties identify a universal computational substrate that all neural models of these structures must satisfy.

In their simplest form, the three computational properties are: a source of noise that energizes the map formation process; a spatial band pass filter that organizes the noise into a spatial map structure; and a normalization rule that constrains how multiple visual features are competitively allocated across the two-dimensional map surface. These rules extend the key observation of Rojer and Schwartz (1990) that the first two rules may be used to generate the map structure of ocular dominance columns, and the related insight of Erwin, Obermayer, and Schulten (1992) that neural models of cortical maps possess ring-shaped Fourier power spectra, given isotropic connection rules. Normalization of cortical response has been considered in a somewhat different context (Swindale, 1992b). Swindale investigated the extent to which model cortex (Swindale, 1992a) minimizes the local variation in the activity of a cortical region. Table 2 shows how various neural models realize these three mapping rules.

Taken together, the three rules allow us to simulate the spatial organization of both cortical ocular dominance columns and orientation columns, as well as their mutual overlap, as these properties have been revealed by experiment using optical imaging techniques (Blasdel, 1992a,b; Obermayer & Blasdel, 1993).

Another class of models that can account for pattern formation in biological systems are reaction-diffusion (RD) equations (Turing, 1952). RD equations define the time derivative of the concentration of a particular morphogen $C(x, y)$ as

$$\frac{dC}{dt} = a^2\nabla^2 C - bC + R \tag{1}$$

where a is the diffusion rate constant, b is the dissipation rate constant, and R is the reaction function governing C and may depend on the concentrations of other morphogens in the system. Witkin and Kass (1991) note that when the effects of R are small, the solution to above the differential equation is a convolution of the initial state of C with a Difference of Gaussians (DOG):

$$C_{t+\Delta t}(x, y) = C_{t_0}(x, y) \otimes G_{\Delta t}. \tag{2}$$

A similar result was used by Swindale (1980) in his model of ocular dominance column formation. Because a convolution with a DOG is a special case of a band pass filter, solutions to these RD equations amount to band pass filtered versions of the initial concentration

TABLE 1
Some Neural Models of Column Formation

Author	Additional Assumptions	Simulations Show
Grossberg (1976a,b)	Line segments as input	Orientation map
Linsker (1986)	None	Orientation selectivity
Meinhardt and Gierer (1974)	None	General pattern formation
Miller (1992, 1994)	None[a]	Orientation map
Miller et al. (1989)	None[b]	Ocular dominance map
Obermayer et al. (1992)	Initial orientation selectivity	Orientation and ocular dominance maps
Swindale (1992a)	Initial orientation selectivity	Orientation and ocular dominance maps
von der Malsburg (1973)	Line segments as input	Orientation map

[a] Miller's model demands on-center and off-center "Mexican-hat" filters of random inputs.
[b] The input is not completely random: there exists same-eye correlation and anticorrelation.

TABLE 2
Mechanisms That Realize Map Formation Rules

Author	Noise Source	Band Pass Filter	Normalization
Grossberg (1976a,b)			
Grossberg and Olson (1994)	Initial orientation preference, eye preference		Explicit
Linsker (1986)	Initial weights, random (uncorrelated input)	Low pass (preferential short range connections from one layer to the next); learning rule generates positive and negative weights	Bound weights between −1 and 1
Meinhardt and Gierer (1974)	Initial responses	Lateral inhibition + short-range autocatalytic activation	Implicit bounded growth of response
Miller (1992, 1994)	Initial weights	DOG input filter, DOG cortical interaction function	Limit or fix total synaptic strength
Miller et al. (1989)	Initial weights	Short-range correlated firing, longer-range uncorrelated firing; DOG cortical interaction function	Limit or fix total synaptic strength
Obermayer et al. (1992)	Initial orientation preference, eye preference	Local excitation, longer range inhibition	Learning law tends to normalize
Rojer and Schwartz (1990)	Initial responses	Explicit	No
Swindale (1992a)	Initial orientation preference, eye preference	Map changes proportional to map convolved with DOG	Limits on dominant values, orientation vectors; competition
Turing (1952)	Initial state of system	Band pass filter is a solution for RD equation with negligible reaction component	Limit to maximum morphogen concentrations
von der Malsburg (1973)	Strength of afferents to excitatory cells	Excitatory and inhibitory cells. Longer range connections from inhibitory cells	Explicit weight normalization

distribution. As long as the effects of the reaction term is small, the RD model of column formation is identical to the bandpass filter model of column formation (Rojer & Schwartz, 1990).

The relationship between RD equations and neural network models was noted by Grossberg (1976a). He pointed out that the two classes of models are computationally equivalent, and that this similarity, among other properties, can help to explain the smooth transition between prenatal and postnatal development and learning (also see Kandel & O'Dell, 1992). Equivalent computations may thus be performed by either chemical or neural systems and both types of systems exhibit properties of a band pass filter.

3. BAND PASS FILTERS

At least three different forms of band pass filters, the GR filter, the DOG filter, and the ideal filter, are sufficient to generate the desired results. These filters may be multiplied with images in the Fourier domain to effect a computation identical to convolution with their spatial kernels.

The Gaussian Ring (GR) filter is defined in the frequency domain, as in Rojer and Schwartz (1990), as a Gaussian-shaped pass band of standard deviation s, centered at mean frequency ω:

$$GR(x) = e^{-((x-\omega)^2/s^2)}. \tag{3}$$

The DOG filter, defined by the convolution kernel

$$h(x, y) = e^{-\{(x^2+y^2)/2s_1^2\}} - e^{-\{(x^2+y^2)/2s_2^2\}}$$

in the spatial domain, becomes

$$\mathrm{DOG}(x, y) = 2\pi\left(s_1^2 e^{-(s_1^2\omega_x^2)/2-(s_1^2\omega_y^2)/2} - s_2^2 e^{-(s_2^2\omega_x^2)/2-(s_2^2\omega_y^2)/2}\right) \tag{4}$$

in the Fourier domain. The ideal filter is simply a step

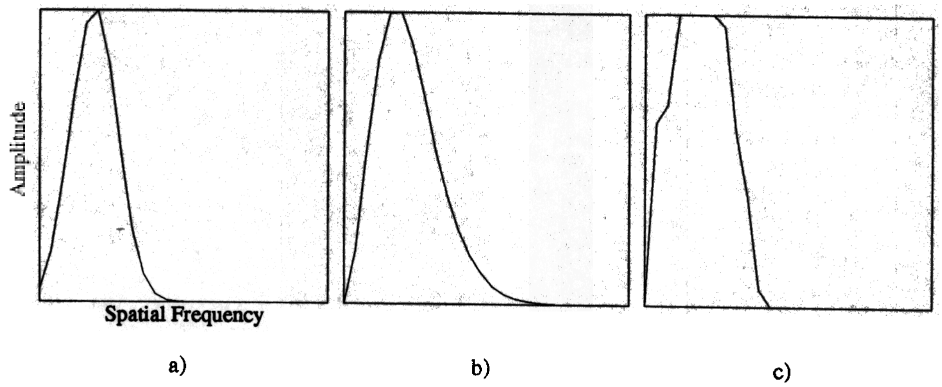

FIGURE 2. Cross sections of the three band pass filters, averaged over all directions. The power of each filter as a function of spatial frequency is shown. (a) GR filter, (b) DOG filter, (c) ideal filter.

function that passes only spatial frequencies that lie within δ of the mean frequency ω:

$$\mathrm{Ideal}(x) = \begin{cases} 1 & \text{if } |x - \omega| < \delta \\ 0 & \text{otherwise.} \end{cases} \tag{5}$$

Figure 2 illustrates the filters defined by eqns (3)–(5) with parameters chosen to emphasize their similarity. These figures are the average cross sections of each of the filters, computed directly from their digital image representations. Due to the discretization of the digital image, the average cross section of the ideal filter does not closely resemble the step function by which it was defined. The circular annulus described by eqn (5) cannot be precisely represented by a discrete rectangular array.

Figure 3 shows the result of applying each band pass filter to the same noise source. Band pass filters that closely resemble one another in the frequency domain thus have a similar effect on noise. The DOG filter is of particular interest because DOG filters and their approximations are used to carry out competitive decision making in essentially all the neural network models.

4. COMPETITIVE NORMALIZATION ACROSS FEATURE DIMENSIONS

A competitive normalization property is found, either explicitly or implicitly, in each of the neural network models sketched above. The models of Linsker (1986), Miller, Keller, and Stryker (1989), and von der Malsburg (1973) include explicit normalization of the adaptive weights that undergo learning. Grossberg (1976a,b), Grossberg and Kuperstein (1986), Kohonen (1989), and Obermayer, Blasdel, and Schulten (1992) present models that obtain normalization as an emergent network property due to the action of lateral inhibition. Normalization is necessary to prevent unbounded weight growth and helps the network to learn a feature map in a stable way.

A normalization constraint can be rationalized in higher dimensional systems if the various feature inputs or "dimensions" interact via a mass action or shunting competitive interaction (Grossberg, 1973). Competitive normalization is shown below to generate a key relationship in the physiological data (Blasdel, 1992a,b): spatial loci that correspond to large values of one dimen-

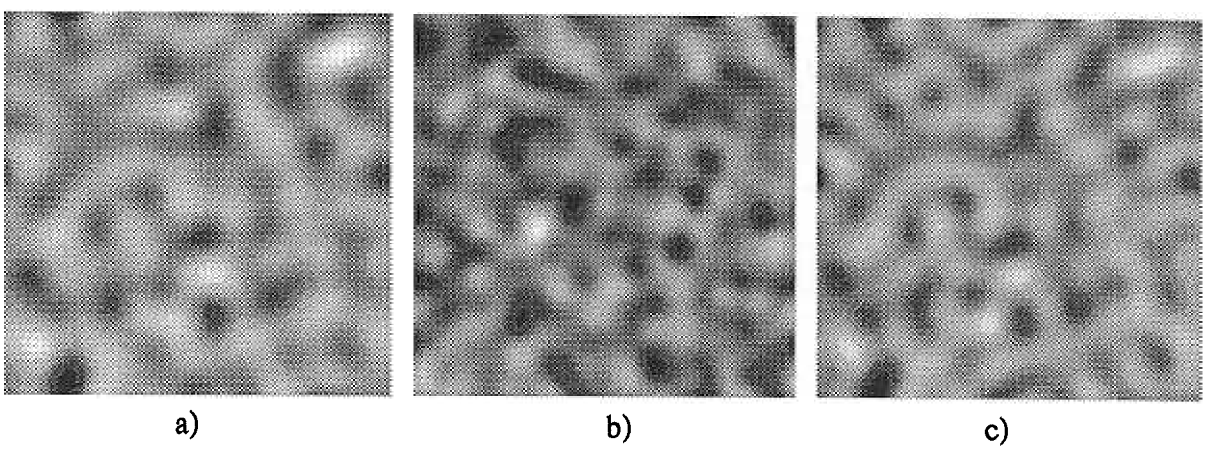

FIGURE 3. Application of each of the band pass filters to an initial two-dimensional noise image. (a) GR filter, (b) DOG filter, (c) ideal filter.

sion correspond to small values of the competing dimension(s). This relationship is expressed by the following equation:

$$\sum_{k=1}^{n} f_k(x_k) = K \tag{6}$$

where each function $f_k(x)$ is an increasing function of x, and K is the maximum response.

5. SIMULATIONS OF CORTICAL MAPS

To simulate cortical maps of orientation and ocular dominance columns we let the number of dimensions $n = 3$, select the transfer function

$$f_k(x) = x^2, \tag{7}$$

and choose $K = 1$. By eqns (6) and (7),

$$x_1^2 + x_2^2 + x_3^2 = 1 \tag{8}$$

which is equivalent to requiring each vector (x_1, x_2, x_3) to lie on the unit sphere. Using these parameters we generate simulated cortical maps with the following procedure (depicted graphically in Figure 4):

- Select two maps of uniformly distributed angles (α, β) which together uniquely determine a single point on the surface of the unit sphere (see Figure 5).
- Coordinates (α, β) correspond to coordinates x_1, x_2, and x_3 such that

$$x_1 = \cos\alpha \cos\beta; \quad x_2 = \sin\alpha \cos\beta; \quad x_3 = \sin\beta \tag{9}$$

  on the unit sphere (8).
- Each image x_1, x_2, and x_3 is band pass filtered to yield simulated response maps y_1, y_2, and y_3. Specifically, each image x_i is transformed into the frequency domain with a fast Fourier transform (FFT), multiplied by the annular-shaped two-dimensional band pass filter, and transformed back into the spatial domain using the inverse FFT. As indicated by the vertical line in Figure 4, there are separate modules for computing ocular dominance and orientation maps. Relaxing the initial constraint that the same filter be used for both systems allows richer model characteristics and closer fits with physiological data.
- We interpret these maps much as Blasdel (1992b) interpreted his physiological data of visual cortex. We take y_1 and y_2 to represent orientation preference and orientation selectivity. At a unique horizontal and vertical position there exists a single scalar value (pixel) in each of the y_1 and y_2 maps, $y_1(h, v)$, and $y_2(h, v)$. The magnitude of the 2-dimensional vector $[y_1(h, v), y_2(h, v)]$,

$$M(h, v) = \sqrt{y_1(h, v)^2 + y_2(h, v)^2} \tag{10}$$

represents orientation selectivity at a given position, and half of the angle of the vector,

$$\theta(h, v) = \text{angle}(y(h, v)) \tag{11}$$

where

$$\text{angle}(z(h, v)) = \text{atan}\left(\frac{z_1(h, v)}{z_2(h, v)}\right) \tag{12}$$

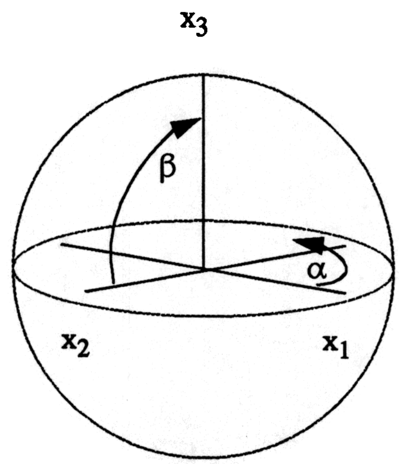

FIGURE 5. Two angles α and β uniquely determine a vector (x_1, x_2, x_3) on the surface of the unit sphere.

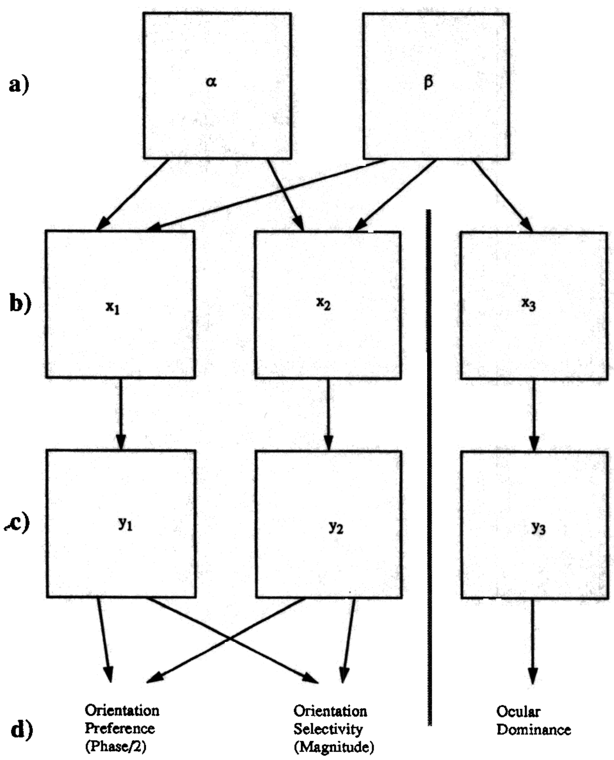

FIGURE 4. (a) Two maps of random angles (α and β) uniquely determine a map of vectors on the unit sphere. (b) The Cartesian coordinates (x_1, x_2, x_3) of each vector are computed from the maps of α and β. (c) A spatial band pass filter is applied to each of the coordinate maps to generate maps of simulated response vectors (y_1, y_2, y_3). (d) Maps y_1 and y_2 are combined to yield maps of orientation preference and orientation selectivity; map y_3 is interpreted as ocular dominance.

represents orientation preference. We restrict the angle to lie between $-\pi/2$ and $\pi/2$ because orientation preference is defined only on this range.

- The final map of eye dominance, E, is represented by y_3:

$$E(h, v) = y_3(h, v) \tag{13}$$

Positive values of $E(h, v)$ represent preference for one eye, and negative values represent preference for the other eye. Values of $E(h, v)$ near 0 represent an absence of eye preference.

6. SIMULATIONS WITH THE SAME FILTER FOR ORIENTATION AND OCULAR DOMINANCE

In order to study this model in some detail, we begin with the restriction that the same filter is applied to all three random maps x_i. We will discuss the strengths and limitations of the model under this restriction before relaxing the constraint to encompass more realistic cases. Figure 6a shows a simulated ocular dominance map. The range $[-1, 1]$ of the E map is shown as a grey-scale image. Light regions correspond to map values near 1 and to regions that "prefer" input from one eye. By contrast dark regions correspond to map values near -1 and to regions that prefer input from the other eye. Grey regions correspond to values near 0 and prefer input from neither eye.

The binocularity map, shown in Figure 6b, is generated by taking the absolute value of each element of the ocular dominance map. Thus regions with values near 0 in the binocularity map correspond to regions that prefer neither eye, and regions with values near 1 in the binocularity map correspond to regions that prefer one eye or the other. This map in the range of $[0, 1]$ is once again shown as a grey-scale image. Light regions show preference to one eye or the other (monocular regions), and dark regions represent approximately equal response to either eye (binocular regions).

Figure 7 shows simulated maps of orientation selectivity. As described above, this map is constructed from the magnitude of the vector $[y_1(h, v), y_2(h, v)]$ for each position (h, v) in the band pass filtered maps y_1 and y_2. Regions with small vector magnitudes correspond to areas of low selectivity: regions that respond equally well to many different orientations. In the orientation selectivity map image these regions are represented as dark regions. Regions with large vector magnitudes correspond to areas of high selectivity, and these sharply tuned regions are represented as light regions in the orientation selectivity map.

One-half of the angle of the vector $[y_1(h, v), y_2(h, v)]$ represents orientation preference in our simulations. Contours of isoorientation preference of a simulated orientation preference map are shown in Figure 8. Notice that this map is qualitatively similar to contour maps of physiologically measured orientation preference, shown in Figure 1. Like the observed map, the simulated map possesses singularities, fractures, and linear zones.

Compare the maps in Figures 6–8. Notice the qualitative similarity between these figures and those of

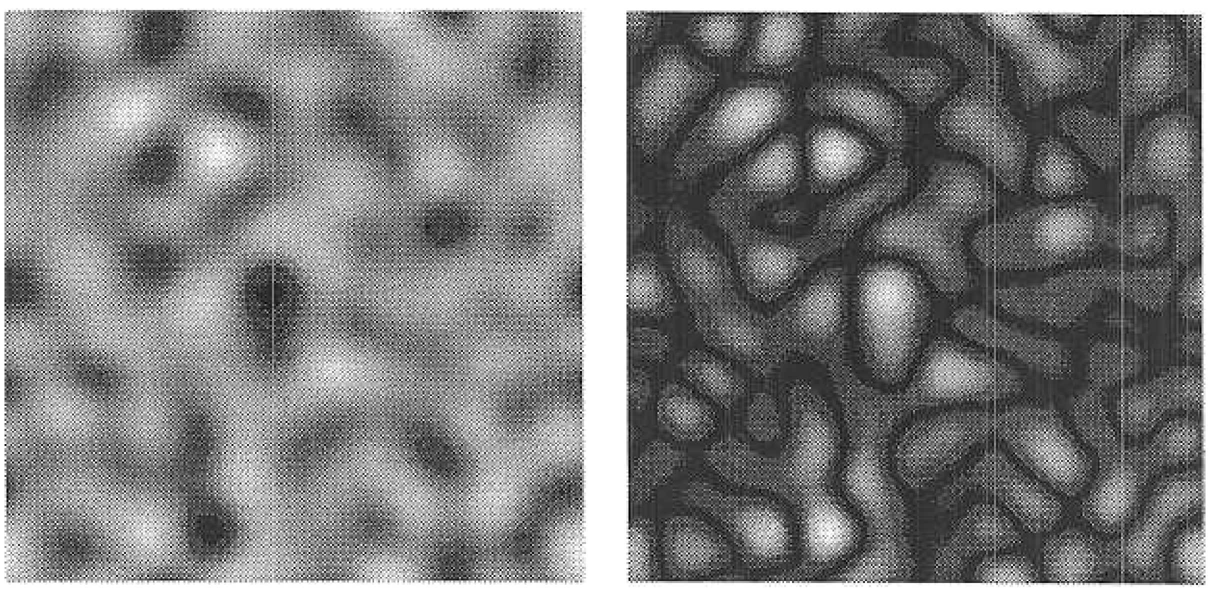

a) b)

FIGURE 6. Two-dimensional maps generated by applying GR filter to normalized random map x_3 (see text). (a) Simulated ocular dominance map y_3. Dark regions correspond to preference for one eye, light regions to preference for the other eye (see text). (b) Simulated binocularity map, absolute value of map y_3. Dark regions correspond to preference for neither eye (binocular regions), light regions to preference for one eye or the other.

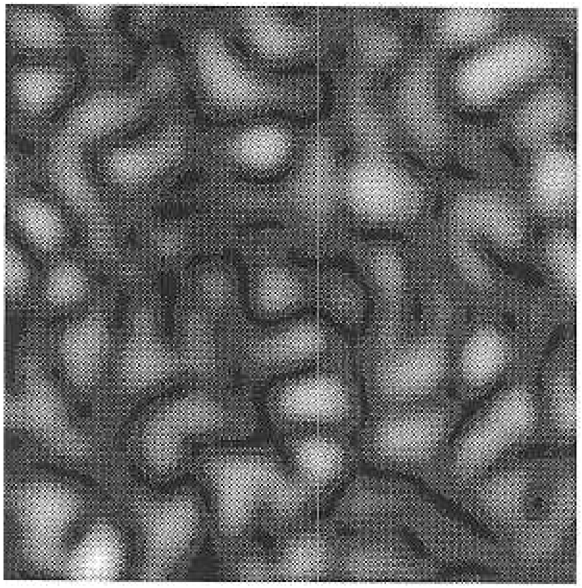

FIGURE 7. Simulated orientation selectivity map extracted from GR-filtered maps. Orientation selectivity is defined as the magnitude of each two-dimensional vector in the map (y_1, y_2). Light regions represent areas of high selectivity, and dark regions represent low selectivity.

physiologically measured maps. In particular notice the existence in the simulated maps of the features of physiological maps identified earlier: linear zones, fractures, and singularities. In addition note that the singularities in the orientation preference map tend to correspond to the centers of the ocular dominance columns, as shown in Figure 9. This is equivalent to the observation that the singularities in the orientation preference map tend to correlate with regions of low binocularity. These qualitative features of these maps are not dependent upon the specific band pass filter used. Our simulations show that simulated cortical maps generated with either the GR filter or the ideal filter are qualitatively similar to the maps shown above.

The fifth property identified by Obermayer and Blasdel (1993) is the tendency of isoorientation contours to intersect ocular dominance contours at right angles. Figure 9 shows simulated orientation contours plotted along with the borders of the simulated ocular dominance columns. By inspection alone, it is unclear if the tendency observed by Obermayer and Blasdel is present in the simulated maps as well. In order to quantify this relationship, we compute the angle of intersection of the maps following the procedure outlined by Obermayer and Blasdel:

- Compute the gradient of the orientation map (also a map). At each position in the map the gradient of orientation is a vector defined by its two components:

$$\nabla\theta_1(h, v) = \theta(h+1, v) - \theta(h-1, v) \qquad (14)$$

$$\nabla\theta_2(h, v) = \theta(h, v+1) - \theta(h, v-1). \qquad (15)$$

We therefore have a map of orientation gradient vectors

$$\nabla\theta(h, v). \qquad (16)$$

- Compute the gradient of the ocular dominance map, resulting in a similar map of ocular dominance gradient vectors

$$\nabla E(h, v). \qquad (17)$$

- Locally average both gradient maps over a "biologically significant" region with radius 100 μm. This appropriate averaging radius for the simulated maps is obtained by requiring that the ratios of the averaging sizes and the average periodicities in the simulated and observed maps be equal. Thus

$$\frac{x}{40 \text{ pixels}} = \frac{100\ \mu\text{m}}{700\ \mu\text{m}}, \qquad (18)$$

which shows that the averaging radius for the simulated maps should be approximately 6 pixels. Maps of averaged gradient vectors

$$\overline{\nabla\theta}(h, v), \overline{\nabla E}(h, v) \qquad (19)$$

are hereby obtained.

- Define P^{OP}, after Obermayer and Blasdel (1993), as the magnitude of the orientation gradient vector, normalized across the entire map:

$$P^{OP} = |\sqrt{\overline{\nabla\theta_1}^2 + \overline{\nabla\theta_2}^2}|. \qquad (20)$$

- Subtract the averaged map of orientation gradient from the averaged map of ocular dominance gradient to yield a map of angular intersection:

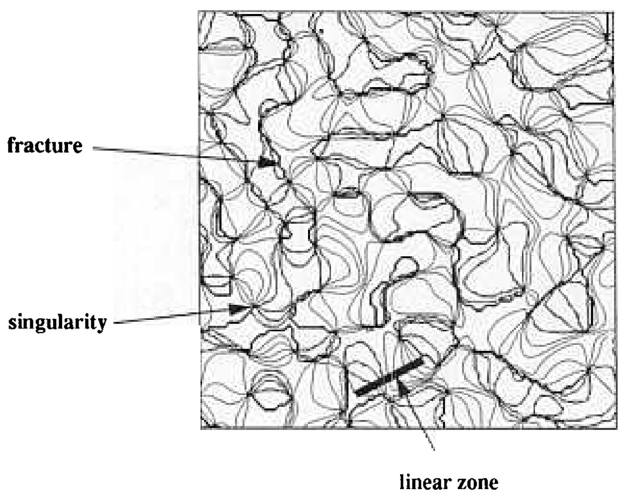

FIGURE 8. Simulated orientation preference map extracted from GR-filtered maps. Orientation preference is defined as half the angle determined by each two-dimensional vector in the map (y_1, y_2). Contour lines are drawn along regions of constant orientation. Examples of a singularity, a fracture, and a linear zone are identified.

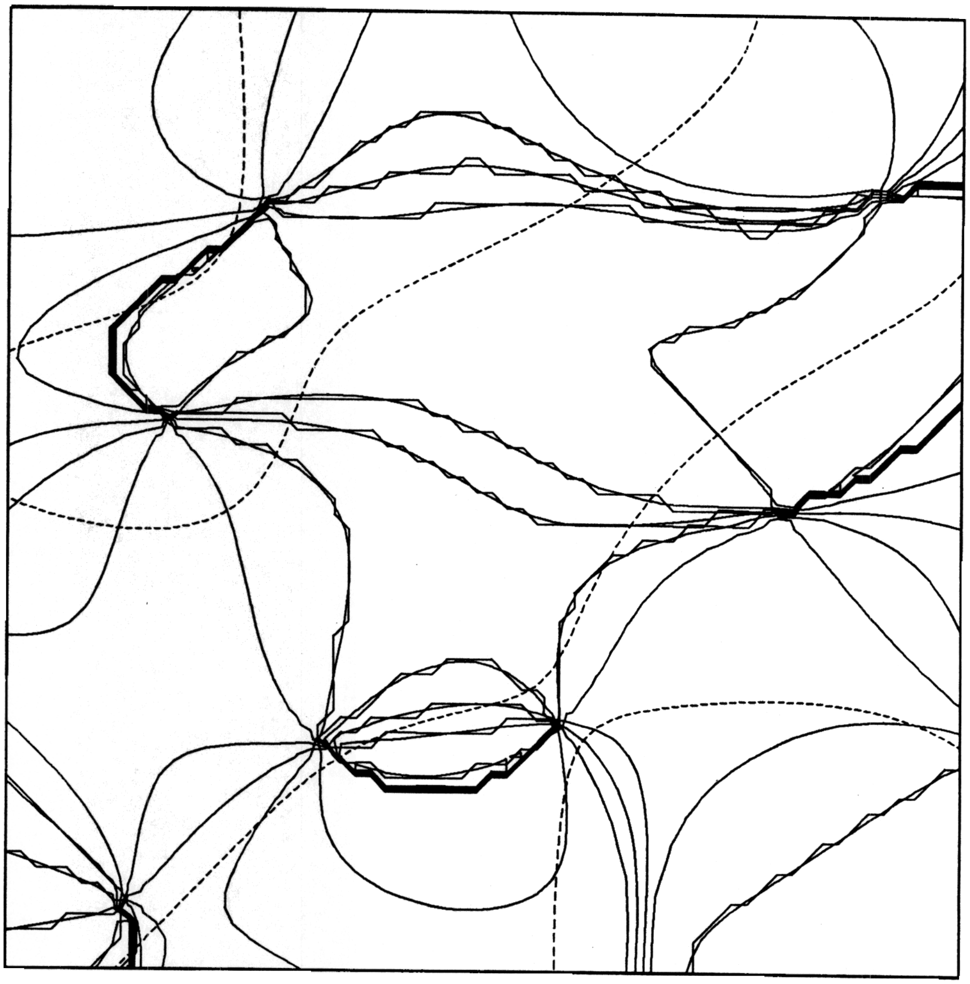

FIGURE 9. Simulated orientation preference contours superimposed on simulated ocular dominance column boundaries (generated with an isotropic filter) do not demonstrate a striking tendency of the contours to intersect the boundaries at right angles. Solid lines show isoorientation contours, dashed lines show boundaries of ocular dominance columns.

$$\gamma(h, v) = \text{angle}(\overline{\nabla\theta}(h, v)) - \text{angle}(\overline{\nabla E}(h, v)). \quad (21)$$

To examine the angle of intersection at different subregions of the simulated maps, the measure of parallelism P^{OP}, defined above, is used to divide the maps into five regions. P^{OP} is small in regions where there is a significant "disagreement" of preferred orientation, and is close to 1.0 in regions where orientation preferences line up with one another.

Figure 10 shows the distribution of P^{OP}. There is obviously a significant bias toward lower values, which translates to a decreased likelihood of strong local "agreement" in the orientation gradient map. Figure 11 shows the distribution of angles of intersection between ocular dominance and orientation gradients, $\gamma(h, v)$, for different values of P^{OP}. In contrast to the physiological maps, which show a tendency for orthogonal intersection of orientation and ocular dominance gradients, the maps generated by the band pass filter model under the restriction of identical orientation and ocular dominance filters show an even distribution of intersection angle.

7. SIMULATIONS WITH ISOTROPIC ORIENTATION FILTER AND ANISOTROPIC OCULAR DOMINANCE FILTER

The restricted model is able to account for the existence of four of the five key qualitative properties of orientation and ocular dominance maps, as described above. However, using an isotropic filter to generate a model ocular dominance map results in a patchy ocular dominance map, rather than a stripe-like map as seen in the physiological maps. The physiologically observed property is also obtained by replacing the isotropic filter that generates the ocular dominance map with an anisotropic filter.

An anisotropic filter was generated by multiplying the annular isotropic filter by a one-dimensional Gaussian:

$$\text{AN}(x, y) = \text{DOG}(x, y)e^{-sy} \quad (22)$$

where the parameter s controls the anisotropy of the filter. This results in a two-lobed filter rather than the

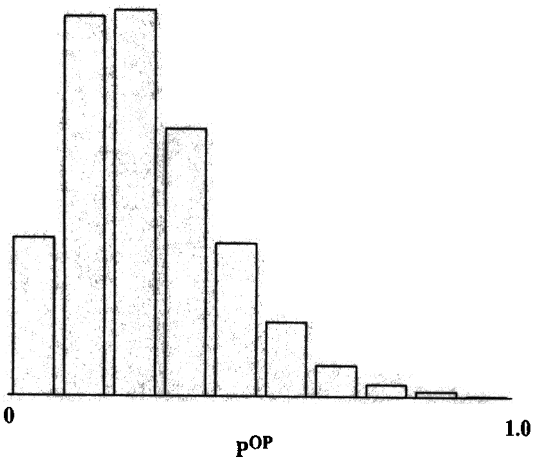

FIGURE 10. Distribution of the (normalized) magnitude of the gradient of orientation preference. The bias toward smaller values is not echoed in the physiological data.

annular isotropic filter. Applying the filter $AN(x, y)$ to the noise source, x_3, as in Figure 4, results in stripe-like map of ocular dominance, which closely resembles macaque ocular dominance maps (Figure 12). This observation was first made by Rojer and Schwartz (1990) who demonstrated that a wide variety of stripe-like patterns could be created by varying the parameters of the filter.

Not only does replacing the isotropic filter with an anisotropic filter yield maps that more closely resemble the patterns observed in monkey cortex, but the previously discussed problem of the orthogonal intersection of orientation and ocular dominance contours is alleviated as well. Figure 13 demonstrates the marked tendency of orthogonal intersection for different values of P^{OP}. This tendency is especially pronounced for higher values of P^{OP}, just as is the case in the physiologically observed maps. Thus it seems that orthogonal intersection emerges from anisotropy in the ocular dominance map.

8. DISCUSSION

All of the properties of orientation and ocular dominance maps identified by Obermayer and Blasdel (1993) can be accounted for by properties of the current model. Thus the characteristics of the physiological maps may be thought of as emerging from the dynamics of a complex self-organizing system that embody the initial disorder, normalization, and filtering properties of the current model.

Singularities are determined by the topology of the interaction of all three components. The x_1 and x_2 maps are selected from orthogonal components of a map of random angles. After filtering, high spatial frequencies are removed, resulting in local spatial correlation. Thus small regions that contain vectors with similar angles will form sharply tuned regions of a specific orientation preference after filtering. In contrast, vectors in small regions with many different angles tend to cancel with one another as a result of filtering, yielding small regions in which the vectors all have small magnitude and many orientations. In a contour plot of orientation preference, these regions show up as singularities, and correspond to regions of low orientation selectivity. Removal of low frequencies leads to a spatial anticorrelation of slightly more distant regions, and increases the regularity of the spatial pattern.

Linear zones and fractures develop according to similar principles. It is helpful to think about fractures and linear zones as the endpoints of a continuum. Similar nearby regions in the initial angular map interact to form regions in the final map with a range of rates of spatial orientation change. Nearby regions with slightly different orientation preferences yield linear zones. Nearby regions with drastically different initial orientation preference form fractures. The initial distribution of angular differences produces the wide range of orientation changes, punctuated by linear zones and fractures, that is seen in simulated maps.

The physiologically observed tendency of orientation preference singularities to lie at the centers of ocular dominance columns is explained by the normalization constraint. Vectors near the centers of ocular dominance columns have large y_3 coordinates and small y_1 and y_2 coordinates; vectors with a small y_3 coordinate have $[y_1, y_2]$ subvectors with large magnitudes. Thus vectors near the centers of orientation columns have small orientation selectivity, a necessary condition for singularities in the orientation preference map. Conversely, vectors away from the centers of orientation columns have larger orientation selectivity: therefore

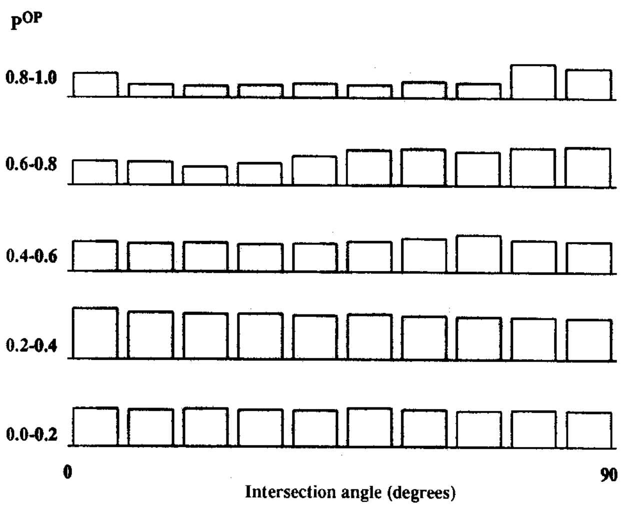

FIGURE 11. Distribution of the angle of intersection for five ranges of P^{OP}. Simulated ocular dominance map was created with an isotropic filter. No tendency toward orthogonal intersection is apparent.

singularities as a rule do not lie away from the centers of the ocular dominance columns.

As described above, orientation contour lines run between pairs of singularities. Because singularities show a strong tendency to line up with the centers of ocular dominance columns, these contour lines are constrained to run from the center of one ocular dominance column to the center of a neighboring column, or roughly along the center line of a single ocular dominance column. It is not well understood why the contours that connect orientation centers exhibit a preference for intersecting the ocular dominance contours at right angles. However, the current model suggests that orthogonal intersection property results from anisotropy in the map of ocular dominance. Based upon this model, we can make the prediction that isotropic ocular dominance systems (such as those in the cat) will not show a tendency toward orthogonal intersection.

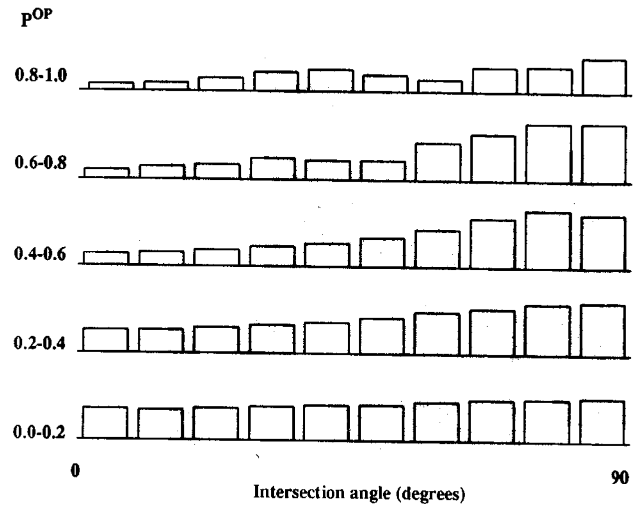

FIGURE 13. Distribution of the angle of intersection for five ranges of P^{OP}. Simulated ocular dominance map was created with an anisotropic filter. For larger values of P^{OP} there is a distinct bias toward orthogonal intersection, as in the physiologically observed maps.

9. CONCLUSION

This conceptually and computationally simple class of models is capable of explaining the key observations made by physiological imaging of primary visual cortex with 2DG and optical recordings. The qualitative structures of the orientation preference, orientation selectivity, and ocular dominance columns emerge, as do the observed topographical relationships among these maps.

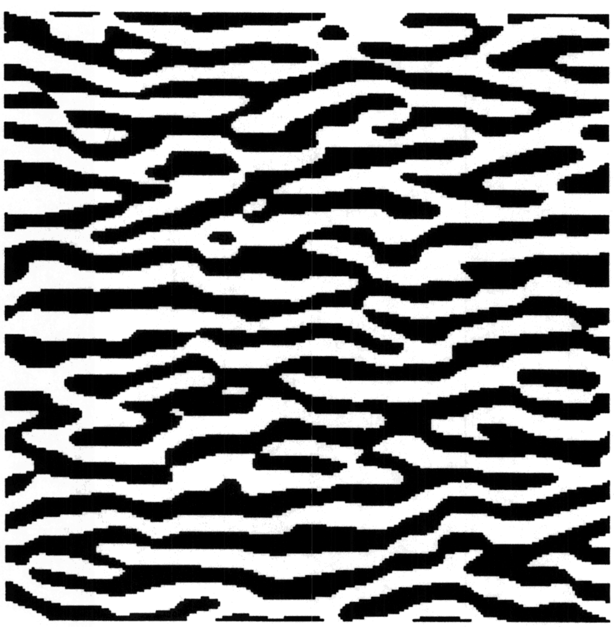

FIGURE 12. Simulated ocular dominance stripes using an anisotropic filter. Continuous map has been thresholded to emphasize difference between eye preference stripes. Light regions represent preference for one eye, dark regions represent preference for the other eye.

The similarity between the synthetic and the experimental maps suggests that the cortex performs a band pass filter of noise and competitive normalization across feature dimensions. Such mechanisms could be due to neural interactions. This is the type of explanation given by all the neural network models reviewed above. On the other hand, other types of mechanisms with similar computational properties could also generate the observed results. In one of the articles that founded the theory of self-organizing cortical feature maps, Grossberg (1976a) noted that model neural mechanisms of postnatal feature map tuning share computational properties with model morphogenetic mechanisms of prenatal feature map formation. These computational homologs enable postnatal map tuning to refine prenatally developed maps in a computationally consistent way. For example, in the morphogenetic models, morphogens cooperate and compete among cells that obey mass action reaction-diffusion equations, thereby achieving competitive normalization. In addition, feature tuning by postnatal mechanisms of activity-dependent synaptic modification obey mathematical rules like those that model prenatal growth of intercellular connections. Similar morphogenetic signals and growth rules are also capable of modeling a variety of nonneural developmental data (Grossberg, 1978).

Our simulation results suggest that whatever combination of genetically and environmentally controlled mechanisms for cortical mapping exists, it needs to incorporate computations that behave like a noise input, a spatial band pass filter, and competitive normalization across feature dimensions. The computational similarity of neural and morphogenetic models also suggest that some of these same properties may be sought in examples of nonneural morphogenetic maps.

REFERENCES

Bienenstock, Cooper, & Munro (1982). Theory for the development of neuron selectivity: Orientation specificity and binocular interaction in visual cortex. *The Journal of Neuroscience*, **2**, 32–48.

Blasdel, G. G. (1992a). Differential imaging of ocular dominance and orientation selectivity in monkey striate cortex. *The Journal of Neuroscience*, **12**(8), 3115–3138.

Blasdel, G. G. (1992b). Orientation selectivity, preference, and continuity in monkey striate cortex. *The Journal of Neuroscience*, **12**(8), 3115–3138.

Blasdel, G., & Salama, G. (1986). Voltage sensitive dyes reveal a modular organization in monkey striate cortex. *Nature*, **321**, 579–585.

Erwin, E., Obermayer, K., & Schulten, K. (1992). *A comparison of models of visual cortical map formation* (Tech. Rep. UIUC-BI-TB-92-16). The University of Illinois.

Grossberg, S. (1972). Neural expectation: Cerebellar and retinal analogs of cells fired by learnable or unlearned pattern classes. *Kybernetik*, **10**, 49–57.

Grossberg, S. (1973). Contour enhancement, short-term memory and constancies in reverberating neural networks. *Studies in Applied Mathematics*, **52**, 217–257. Reprinted in S. Grossberg, (1982). *Studies of mind and brain*. Dordrecht: Kluwer Academic Publishers.

Grossberg, S. (1976a). On the development of feature detectors in the visual cortex with application to learning and reaction-diffusion systems. *Biological Cybernetics*, **21**, 145–159.

Grossberg, S. (1976b). Adaptive pattern classification and universal recoding I: Parallel development and coding of neural feature detectors. *Biological Cybernetics*, **23**, 121–134.

Grossberg, S. (1978). Communication, memory, and development. In R. Rosen and F. Snell (Eds.) *Progress in theoretical biology*. Vol. 5, New York: Academic Press.

Grossberg, S., & Kuperstein, M. (1986). *Neural dynamics of adaptive sensory-motor control*. Amsterdam: Elsevier; Expanded Edition. New York: Pergamon (1989).

Hubel, D. H., & Wiesel, T. N. (1974). Sequence regularity and geometry of orientation columns in the monkey striate cortex. *Journal of Comparative Neurology*, **158**, 267–293.

Hubel, D., Wiesel, T., & LeVay, S. (1977). Plasticity of ocular dominance columns in monkey striate cortex. *Philosophical Transactions of the Royal Society of London Series B*, **278**, 131–163.

Hubel, D., Wiesel, T., & Stryker, M. (1978). Anatomical demonstration of orientation columns in macaque monkey. *Journal of Comparative Neurology*, **177**, 361–380.

Humphrey, A., & Hendrickson, A. (1983). Background and stimulus-induced patterns of high metabolic activity in the visual cortex (area 17) of the squirrel and macaque monkey. *The Journal of Neuroscience*, **3**, 345–358.

Kandel, E. R., & O'Dell, T. J. (1992). Are adult learning mechanisms also used for development? *Science*, **258**, 243–245.

Kohonen, T. (1989). *Self-organization and associative memory* (3rd ed.). New York: Springer–Verlag.

LeVay, S., Connolly, M., Houde, J., & Van Essen, D. (1985). The complete pattern of ocular dominance stripes in the striate cortex and visual field of the macaque monkey. *The Journal of Neuroscience*, **5**(2), 486–501.

LeVay, S., Hubel, D., & Wiesel, T. (1975). The pattern of ocular dominance columns in macaque visual cortex revealed by a reduced silver stain. *Journal of Comparative Neurology*, **159**, 559–576.

Linsker, R. (1986). From basic network principles to neural architecture: Emergence of spatial-opponent cells. *Proceedings of the National Academy of Sciences*, 7508–7512.

Meinhardt, H., & Gierer, A. (1974). Applications of a theory of biological pattern formation based on lateral inhibition. *Journal of Cell Science*, **15**, 321–346.

Miller, K. (1992). Development of orientation columns via competition between on- and off-center inputs. *NeuroReport*, **3**(1), 73–76.

Miller, K. (1994). A model for the development of simple cell receptive fields and the ordered arrangement of orientation columns through activity-dependent competition between on- and off-center inputs. *The Journal of Neuroscience*, **14**(1), 409–441.

Miller, K., Keller, J., & Stryker, M. (1989). Ocular dominance column development: Analysis and simulation. *Science*, **245**, 605–615.

Obermayer, K., & Blasdel, G. G. (1993). Geometry of orientation and ocular dominance columns in monkey striate cortex. *The Journal of Neuroscience*, **13**(10), 4114–4129.

Obermayer, K., Blasdel, G. G., & Schulten, K. (1992). Statistical-mechanical analysis of self-organization and pattern formation during the development of visual maps. *Physical Review A*, **45**(10), 7568–7589.

Rojer, A., & Schwartz, E. (1990). Cat and monkey cortical columnar patterns modeled by band-pass-filtered 2d white noise. *Biological Cybernetics*, **62**, 381–391.

Swindale, N. (1980). A model for the formation of ocular dominance column stripes. *Proceedings of the Royal Society of London Series B*, **208**, 243–264.

Swindale, N. (1992a). A model for the coordinated development of columnar systems in primate striate cortex. *Biological Cybernetics*, **66**, 217–230.

Swindale, N. (1992b). Coverage and design of striate cortex. *Biological Cybernetics*, **66**, 415–424.

Turing, A. (1952). The chemical basis of morphogenesis. *Philosophical Transactions of the Royal Society of London Series B*, **237**, 37–72.

Tootel, R., Hamilton, S., Silverman, M., & Switkes, E. (1988a). Functional anatomy of macaque striate cortex. I. Ocular dominance, binocular interactions, baseline conditions. *The Journal of Neuroscience*, **8**, 1500–1530.

von der Malsburg, C. (1973). Self-organization of orientation sensitive cells in the striate cortex. *Kybernetik*, **14**, 85–100.

Willshaw, D. J., & von der Malsburg, C. (1976). How patterned neural connections can be set up by self-organization. *Proceedings of the Royal Society of London (B)*, **194**, 431–445.

Witkin, A., & Kass, M. (1991). Reaction diffusion textures. *Computer Graphics (SIGRAPH)*, **25**(4), 299–307.